Scripta Materialia 123 (2016) 13–16

Contents lists available at ScienceDirect

Scripta Materialia

journal homepage: www.elsevier.com/locate/scriptamat

Regular Article

Interface controlled microstructure evolution in nanolayered thin films

M. Bartosik [a,*], J. Keckes [b], P.O.Å. Persson [c], H. Riedl [a], P.H. Mayrhofer [a]

[a] Institute of Materials Science and Technology, TU Wien, Austria
[b] Department of Materials Physics, Montanuniversität Leoben, Austria
[c] Department of Physics Chemistry and Biology, Linköpings Universitet, Sweden

ARTICLE INFO

Article history:
Received 17 March 2016
Received in revised form 21 May 2016
Accepted 22 May 2016
Available online 7 June 2016

Keywords:
Coherent
Incoherent
Interfaces
Microstructure
Multilayer

ABSTRACT

X-ray nano-diffraction and transmission electron microscopy were conducted along the thickness of a ~4 μm thick CrN/AlN multilayer with continuously increasing AlN layer thicknesses from ~1 to 15 nm on ~7 nm thick CrN template layers. The experiments reveal coherent growth, large columnar grains extending over several (bi-)layers for thin AlN layer thicknesses below ~4 nm. Above ~4 nm, the nucleation of the thermodynamically stable wurtzite structured AlN is favored, leading to coherency breakdown and reduction of the overall strains, disrupting the columnar microstructure and limiting the maximum grain size in film growth direction to the layer thickness.

Thin films synthesized by physical or chemical vapor deposition techniques often show a strong microstructural dependence of their properties [1]. The electrical and thermal conductivity, for instance, decreases with decreasing grain size as the grain boundaries act as scattering centers for electrons and/or phonons [2]. The thermal expansion, on the other hand, increases with decreasing grain size as the volume content of grain boundaries and therefore the amount of weakly bonded atoms increases [3]. The hardness and yield stress attain maximum values for a critical minimum grain size corresponding to the Hall-Petch relation [1]. Consequently, optimizing film properties requires a detailed understanding of the mechanisms that influence the microstructure evolution during film growth.

For monolithic films (we use this term to separate them from multilayers as monoliths can also contain several grains as thin films in general), structure zone models [4–7] describe the crystallite size and shape evolution for prevailing film deposition conditions. For multilayer films composed of nm-thin individual layers it is known that the limited thickness may be used to epitaxially stabilize metastable phases and to form coherent interfaces [8]. However, although having attracted much scientific interest due to their outstanding mechanical [9] and tribological properties [10], only little information is available on how the film deposition conditions – the (bi-)layer period and in particular the interface type between consecutive layers (coherent, semi-coherent, incoherent) – influence the microstructure evolution.

Here we use wide angle X-ray nano-diffraction to reconstruct the crystallite size and shape along the film thickness of a CrN/AlN nanolayered film, where the growth mode of the individual layers was changed from coherent to incoherent in the course of the deposition process. The results are cross-validated and complemented by independent transmission electron microscopy (TEM) investigations. In the last section of this article, implications of the interface-type-related microstructure formation on the film properties are briefly discussed.

A ~4 μm thick CrN/AlN multilayer was deposited in an AJA Orion 5 laboratory-scale unbalanced magnetron sputter system equipped with a three-inch Al and a two-inch Cr target (both from Plansee Composite Materials GmbH, 99.6 purity). Prior to the deposition, the substrates were ultrasonically cleaned for 5 min in ethanol and acetone, respectively, thermally cleaned at 500 °C for 20 min (within the deposition chamber at a base pressure below 0.1 MPa) and Ar-ion etched (gas pressure = 6 Pa) at the same temperature for 10 min. During the deposition, the substrate temperature was kept constant at 500 °C and the substrates were rotated with 1 Hz. The deposition was performed in an Ar/N_2 gas mixture with a flow rate ratio of 3/2 and a total pressure of 0.4 Pa. A bias voltage of −50 V was applied to the substrates to ensure a dense film morphology. The Al and Cr targets were dc-powered using a target power density of 10 and 12 W/cm^2, respectively. The AlN layer thicknesses were intentionally increased from ~1 to 15 nm while keeping the CrN layer thicknesses constant at ~7 nm using a computer controlled shutter system. The increase of the AlN layer thickness was intended to result in a change of the growth mode from coherent to incoherent between CrN and AlN layers along the multilayer stack. In preparation for the nano-diffraction experiment, a ~50 μm thick lamella

* Corresponding author.
E-mail address: matthias.bartosik@tuwien.ac.at (M. Bartosik).

http://dx.doi.org/10.1016/j.scriptamat.2016.05.031

was prepared form the as-deposited samples by mechanical grinding and polishing.

The nano-diffraction experiment was conducted in the nano-focus endstation of the ID13 beamline at the European Synchrotron Radiation Facility in Grenoble (France). The experimental setup is schematically shown in Fig. 1. The film was characterized in transmission geometry by position-resolved wide angle X-ray diffraction (WAXD) using a monochromatic X-ray beam with an incident energy of ~14.9 keV, nano-focused to ~80 nm in diameter with Kirkpatrick-Baez (KB) mirror optics. The specimen was aligned so that the film-substrate interface was oriented parallel to the incoming beam and moved stepwise in vertical direction with a step width of 50 nm. A Charge-Coupled Device area detector (Eiger 4 M), placed at a distance of ~10.6 cm behind the specimen, recorded characteristic Debye-Scherrer diffraction patterns from different film depths with a counting time of ~0.6 s per frame. More details on the experimental approach can be found in Refs. [11, 12].

The change of the interface type from coherent to incoherent along the CrN/AlN multilayer thickness was determined from the wide angle diffraction patterns. The contour plot presented in Fig. 2 shows the intensity vs. 2θ dependence of the integrated WAXD patterns as a function of film thickness. For a total film thickness below ~0.6 μm only diffraction peaks from the face-centered cubic crystal structure are present. This suggests coherent growth between B1-CrN and AlN stabilized by CrN (template) layers in its metastable B1 structure. Based on our cross-sectional TEM investigations (see further below), this condition is persistent for AlN layer thicknesses below ~4 nm, which corresponds to an integrated multilayer thickness up to ~0.6 μm. For AlN layers thicker than ~4 nm, additional wurtzite-related reflections are detected indicating a loss of coherency and growth of AlN in its thermodynamically stable B4 crystal structure. The relative change in intensity of the 111 and 200 reflections along the film thickness indicate a crystallographic texture cross-over from 200 to 111 preferred orientation.

The reason for the coherency break down was demonstrated by the model from Chawla et al. [13] for cubic AlN in CrN/AlN and TiN/AlN bilayer systems. The authors calculated the elastic strain energy stored in the system due to the coherent but lattice mismatched interface between (cubic, wurtzite) AlN and underlying CrN using the finite element method and combined it with the chemical and surface energies obtained from first principles. They found, that cubic AlN is energetically favored up to a critical thickness. The thicker the AlN layer, the more relaxed it is due to surface relaxations. Consequently, the contribution of the strain energy to the total energy becomes less important and the thermodynamically stable wurtzite AlN forms.

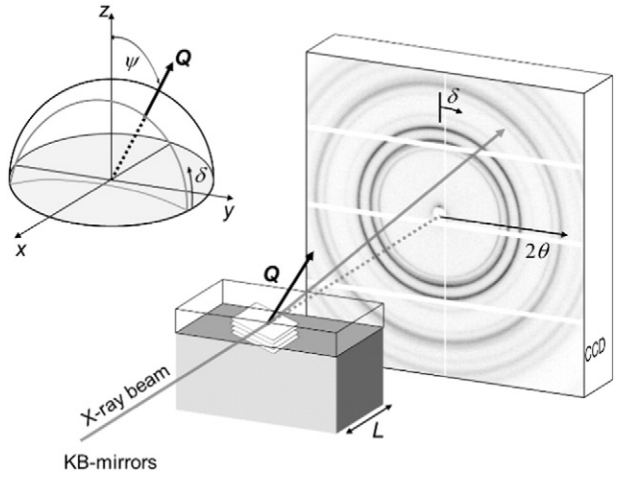

Fig. 1. Schematic representation of the cross-sectional X-ray nano-diffraction experiment carried out in transmission geometry using a monochromatic X-ray beam focused down to submicron dimensions with KB-mirrors. More details can be found in Ref. [11].

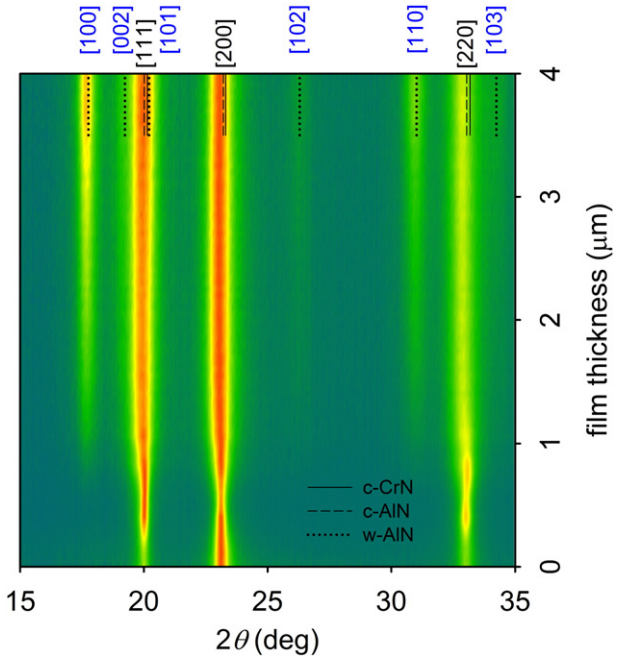

Fig. 2. Intensity vs. 2θ dependence of the integrated WAXD patterns (10° cake integration around $\delta = 90°$). In the case of coherent growth only B1 reflections are visible as AlN is stabilized in its metastable B1 structure by local epitaxy to B1-CrN, while in the case of incoherent growth, B1 and B4 reflections are detected as AlN crystallizes in its thermodynamically stable B4 structure.

Fig. 3a presents the in-plane residual strain evolution along the thickness of our model film, which was evaluated from the elliptical distortion of the cubic (200) Debye Scherrer rings according to Refs. [11, 14]. Following a similar argumentation as Chawla et al. [13], we propose the following explanation for the residual strain data: The coherency strains in the cubic phase(s) increase with increasing AlN layer thicknesses until the critical maximum AlN layer thickness t_{crit} – up to which AlN is fully stabilized in the cubic crystal structure – is reached (t_{crit} ~ 4 nm corresponding to the total film thickness of about ~0.6 to 0.8 μm). While the relative stain increase is more pronounced for very thin AlN layer thicknesses, the slope of the curve decreases for thicker AlN layer thicknesses. With further increase of the AlN layer thicknesses, the strains decrease and level at a constant value. The decrease suggests for strain relaxation events due to ongoing nucleation of the thermodynamically stable wurtzite AlN, compare Figs. 2, 3a) and b).

The coherency breakdown leads to a characteristic microstructure evolution in the coherent and incoherent film regions as discussed in the following. The crystallite size and shape evolution throughout the multilayer film thickness was estimated from the peak broadening along the Debye-Scherrer diffraction rings as a function of the film thickness. The full width at half maximum (FWHM) of the diffraction peaks is a measure for the peak broadening and depends on the crystallite size, strains of second and third order as well as instrumental broadening. When attributing (in a first approximation) the peak broadening to the finite crystallite size only, the coherently diffracting domain size D can be estimated using the Scherrer formula [17,18]

$$D \sim \frac{K\lambda}{\mathrm{FWHM} * \cos\theta}, \quad (1)$$

where K denotes the shape factor, λ the X-ray wavelength, and FWHM the line broadening in radians. The coherently diffracting domain (crystallite) shape was reconstructed by evaluating the FWHM as a function of ψ, whereby the latter denotes the angle between the sample normal and the diffraction vector. The correlation between ψ and the azimuthal angle δ is given by $\cos\psi = \cos\delta\cos\theta$. Consequently, the values $D_{\psi=}$

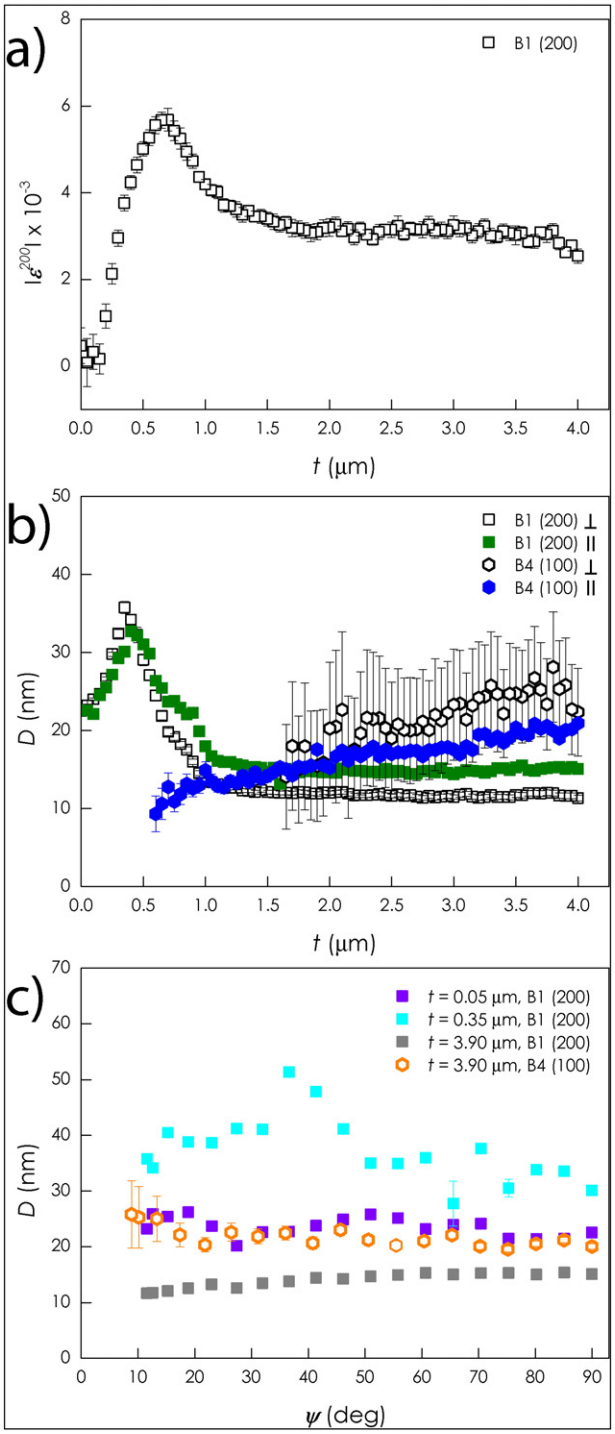

Fig. 3. a) In-plane residual strain evolution $|\varepsilon^{200}|$ (absolute values) in the cubic phase(s) along the CrN/AlN multilayer film thickness where the interface type changes from coherent to incoherent in the course of the PVD process (with the transition starting at ~0.6 μm total film thickness). In b) and c), the coherently diffracting domain size and shape evolution are shown, respectively.

$_{0°} \equiv D_{\perp}$ corresponds to the mean coherently diffracting domain size (crystallite height) in film growth direction and $D_{\psi=90°} \equiv D_{\parallel}$ to that in film in-plane direction.

The results presented in Fig. 3b) indicate a fine-grained film structure near the film-substrate-interface, due to a high number of different nuclei, when there is no epitaxial match between film and substrate. With increasing film thickness, the initially globular grains ($D_{\perp} \sim D_{\parallel}$) become elongated in film growth direction ($D_{\perp} > D_{\parallel}$), gain in size and extend over several CrN and AlN layers ($D_{\perp}$>bilayer thickness). A more detailed evaluation of D as a function of ψ, given in Fig. 3c), suggests that cone-like columnar grains (cyan square symbols) developed on top of an equi-axed fine-grained (violet square symbols) film region in the course of the film growth. Consequently, the multilayer film region with coherently growing AlN layers exhibit a typical "zone T" microstructure according to the zone classification proposed by Thornton [5]. The latter is characterized by a competitive growth where energetically or kinetically favored grains gradually overgrow less favored grains. A similar microstructure was observed for monolithically grown CrN grown under the same deposition conditions (not shown). Hence, we can conclude that the insertion of thin AlN layers, which nucleate coherently on the CrN, do not significantly modify the film microstructure.

In Fig. 3b), along with the coherent-to-incoherent interface type transition (at a total film thickness of ~0.6 μm), a steep decrease of the B1-CrN (plus B1-AlN) coherently diffracting domain size in film growth direction (black open square symbols), leveling out at a constant D value of ~11 nm can be observed. This should be compared to the CrN layer thickness of ~7 nm (plus the ~4 nm thick coherently grown B1-AlN), which was kept constant throughout the entire CrN/AlN multilayer. The B1-CrN crystallites become even broader in in-plane direction than in film growth direction in the incoherently grown multilayer film region (compare full green square with open black square symbols at $t > 0.6$ μm in Fig. 3b), and see the full gray square symbols in Fig. 3c)). Thus, there is a transition of the average crystallite aspect ratio from $D_{\perp}/D_{\parallel} > 1$ to < 1. In the case of B4-AlN, the grains initially do not exist or the grain size in film growth direction (open black hexagon symbols in Fig. 3b)) are below the detection limit for X-ray diffraction. With increasing AlN layer thicknesses, the grains gain in size and become ever larger. Similarly, the in-plane grain size (full blue hexagon symbols in Fig. 3b)) gradually increases.

The findings from the nano-diffraction experiment are cross-validated and complemented by cross-sectional TEM investigations performed on the Linköping double corrected and monochromated Titan^3. An overview high angle annular dark field scanning transmission electron microscopy (HAADF-STEM) image of the entire multilayer stack is presented in Fig. 4a) using an imaging condition to strongly promote diffraction contrast. Areas used for imaging in b–e are schematically identified in a). From the overview image in a), one can clearly identify the layered structure throughout the film thickness, where the CrN layers are bright in this imaging condition. Additionally, at the bottom of the image, one may observe bright columns extending in the growth direction slightly above the substrate–film interface. These bright columns are identified as coherently grown material with common diffraction behavior and extend 0.6–0.8 μm above the interface. Since these columns gradually increase their width during growth, they are supposedly the result of competitive growth. The coherent growth is rather quickly cancelled upon reaching the maximum height. In the proceeding growth, the film does not show any such coherent growth behavior, which is seen by the homogeneous contrast. Investigating the multilayer structure further at higher magnifications by TEM, (b–e) and starting with the thin (and brighter) AlN layers in e), one immediately observes coherent growth. In the middle of Fig. 4e) a column is observed to grow through the image. It is worth noting that the lattice is of a cubic appearance and is perfectly continued from CrN to AlN during growth. At this stage of growth, the column is only ~10 nm wide, therefore additional columns of other orientations are observed adjacent to the central one. In Fig. 4d), the growing column is at its maximum width and the CrN to AlN transition remains coherent and perfectly seamless. As the AlN layer thickness increases to ~6 nm, coherency breaks down, and the result is shown in Fig. 4c). The initial observation is, that the structure now has the appearance of individual grains, with grain size approximately corresponding to the layer thickness. Additionally, one can observe that the AlN layer starts to assume a wurtzite appearance (zig-zag pattern, middle-right). Locally however, the structure appears

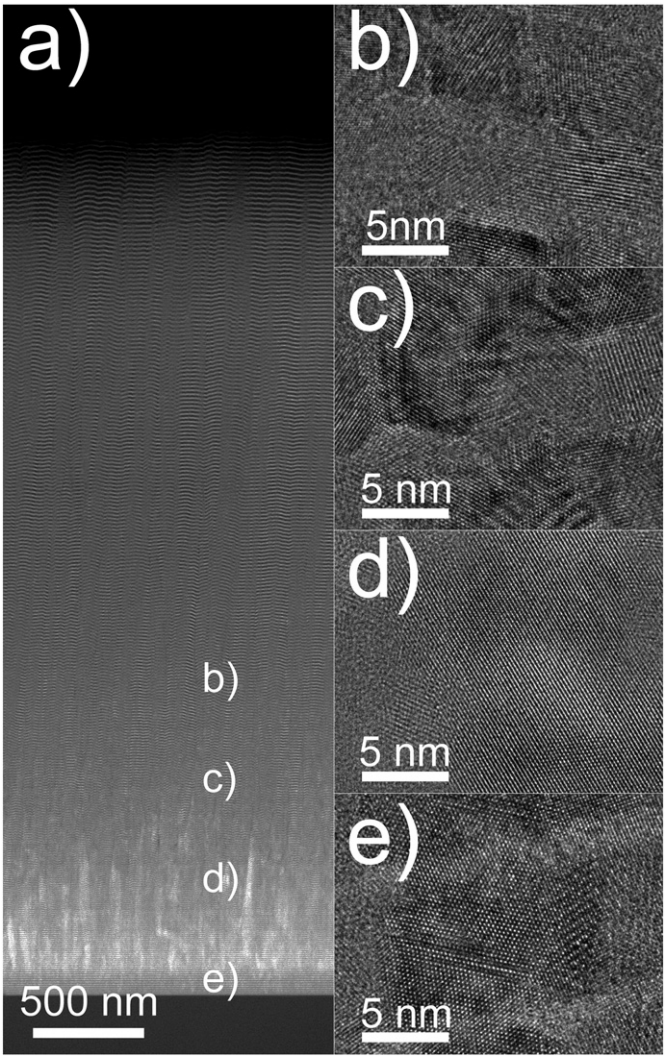

Fig. 4. HAADF-STEM image of the entire CrN/AlN multilayer stack a), where locations for figures (b–e) are schematically identified. The transition from coherent to incoherent growth is shown from the (coherently grown) bottom of the stack in e) to the incoherently grown polycrystalline structure in b).

to exhibit some coherency since the middle-upper and middle-bottom CrN particles exhibit the same lattice orientation. The end result is shown in Fig. 4b) where AlN and CrN particles exhibit the same size as the layer thickness and all particles are individually rotated. A final observation can be made regarding the layer quality. The originally flat layers as observed in Fig. 4e) increasingly accumulate roughness. While the layers are always well defined, even for the topmost layers, the local curvature of the layer may be on the same order as the layer thickness. These undulations (which we also observed in our previous studies on the same multilayer material system [16]) may (at least partly) define the in-plane grain size.

The interface-type-related microstructure evolution will strongly influence the film properties. The thermal conductivity, for instance, is strongly grain size dependent [19,20] and can be modified over several orders of magnitude by controlling the layer thickness and interface type. In addition to the average thermal conductivity, its direction dependence may change from isotropic, for an equi-axed microstructure (and intrinsically isotropic materials), to highly anisotropic when the film forms a columnar microstructure. For the latter, the thermal conductivity is expected to be higher in the film growth direction as compared to the in-plane direction when assuming that the grain boundaries represent a limiting factor for thermal conductivity in thin films. The film microstructure may also play a crucial role for diffusion processes occurring in various applications (e.g., diffusion of oxygen from the atmosphere into the film [21], out-diffusion of nitrogen originating from thermally activated dissociation processes of nitride based films affecting their thermal stability [22], etc.). The deformation and fracture mechanisms of thin films under mechanical load(s) are also influenced by the microstructure [23], to name just a few examples.

Based on our detailed investigations we can conclude that nanometer thick phases are stabilized in their metastable crystal structure by local coherency to template layers. As soon as the thermodynamically stable wurtzite AlN nucleates (for AlN layer thicknesses above ~ 4 nm), the overall strains decrease and level at a constant value. This, in turn, significantly influences the microstructure evolution: While in the coherently grown film regions large columnar grains are observed, which extend over several layers (similar to monolithic films grown under the same deposition conditions), the grain size in film growth direction of incoherently grown film regions is limited by the layer thicknesses. The in-plane grain size of the latter is (at least partly) defined by undulations of the layer structure. The interface-type-related microstructure evolution determines the properties and thus the performance of thin films. Consequently, interface design is crucial in optimizing thin films for various applications.

Acknowledgements

The experiment was performed on beamline ID13 at the European Synchrotron Radiation Facility (ESRF), Grenoble, France. We are grateful to Dr. Manfred Burghammer at the ESRF for providing assistance in using beamline ID13. The financial support by the START Program (Y371) of the Austrian Science Fund (FWF) is gratefully acknowledged. POÅP would like to acknowledge the Swedish Research Council for funding under grants no. 621-2012-4359 and 622-2008-405 as well as the Knut and Alice Wallenberg's Foundation for support of the electron microscopy laboratory in Linköping.

References

[1] P.H. Mayrhofer, C. Mitterer, L. Hultman, H. Clemens, Prog. Mater. Sci. 51 (2006) 032.
[2] T.M. Tritt, Thermal Conductivity: Theory, Properties, and Applications, Kluwer Academic/Plenum Publishers, New York, 2004.
[3] R. Daniel, D. Holec, M. Bartosik, J. Keckes, C. Mitterer, Acta Mater. 59 (2011) 6631.
[4] B.A. Movchan, A.V. Demchishin, Phys. Met. Metallogr. 28 (1969) 83.
[5] J.A. Thornton, J. Vac. Sci. Technol. 11 (1974) 666.
[6] R. Messier, A.P. Giri, R.A. Roy, J. Vac. Sci. Technol. A 2 (1984) 500.
[7] A. Anders, Thin Solid Films 518 (2010) 4087.
[8] H. Söderberg, P.O.Å. Persson, M. Beckers, A. Flink, J. Birch, L. Hultman, M. Odén, J. Mater. Res. 22 (2007) 3255.
[9] U. Helmersson, S. Todorova, S.A. Barnett, J.-E. Sundgren, L.C. Markert, J.E. Greene, J. Appl. Phys. (1987) 62.
[10] P.C. Yashar, W.D. Sproul, Vacuum 55 (1999) 179.
[11] J. Keckes, M. Bartosik, R. Daniel, C. Mitterer, G. Maier, W. Ecker, J. Vila-Comamala, C. David, S. Schoeder, M. Burghammer, Scr. Mater. 67 (2012) 748.
[12] M. Bartosik, R. Daniel, C. Mitterer, I. Matko, M. Burghammer, P.H. Mayrhofer, J. Keckes, Thin Solid Films 542 (2013) 1.
[13] V. Chawla, D. Holec, P.H. Mayrhofer, J. Phys. D. Appl. Phys. 46 (2013) 045305.
[14] M. Bartosik, M. Arndt, R. Rachbauer, C. Krywka, C.M. Koller, J. Keckes, P.H. Mayrhofer, Scr. Mater. 107 (2015) 153.
[16] M. Bartosik, M. Todt, D. Holec, J. Todt, L. Zhou, H. Riedl, H.J. Böhm, F.G. Rammerstorfer, P.H. Mayrhofer, Appl. Phys. Lett. 107 (2015) 071602.
[17] P. Scherrer, Göttinger Nachr. 2 (1918) 98.
[18] A.L. Patterson, Phys. Rev. 56 (1939) 978.
[19] H. Dong, B. Wen, R. Melnik, Sci. Rep. 4 (2014) 7037.
[20] J.P. Feser, E.M. Chan, A. Majumdar, R.A. Segalman, J.J. Urban, Nano Lett. 13 (2013) 2122.
[21] J. Musil, Surf. Coat. Technol. 207 (2012) 50.
[22] W. Ernst, J. Neidhardt, H. Willmann, B. Sartory, P.H. Mayrhofer, C. Mitterer, Thin Solid Films 517 (2008) 568.
[23] I.A. Ovid'ko, in: A. Cavaleiro, J.T.M. De Hosson (Eds.), Nanostructured Coatings, Springer, New York 2006, pp. 78–108.